Optical Materials 82 (2018) 1–6

Contents lists available at ScienceDirect

Optical Materials

journal homepage: www.elsevier.com/locate/optmat

Up-conversion luminescence of $GdVO_4:Nd^{3+}/Er^{3+}$ and $GdVO_4:Nd^{3+}/Ho^{3+}$ phosphors under 808 nm excitation

Dragana J. Jovanović[a,*], Tamara V. Gavrilović[a,b], Slobodan D. Dolić[a], Milena Marinović-Cincović[a], Krisjanis Smits[b], Miroslav D. Dramićanin[a]

[a] Vinča Institute of Nuclear Sciences, University of Belgrade, P.O. Box 522, 11001 Belgrade, Serbia
[b] Institute of Solid State Physics, University of Latvia, 8 Kengaraga Street, Riga, LV 1063, Latvia

ARTICLE INFO

Keywords:
Up-conversion
Gadolinium vanadate
$GdVO_4:Er^{3+}/Nd^{3+}$
$GdVO_4:Ho^{3+}/Nd^{3+}$
808-nm excitation

ABSTRACT

In recent years, there exists a tendency in research of up-conversion materials to shift excitation from 980 nm to shorter wavelengths. Here, in order to produce up-conversion luminescence emission of $GdVO_4$-based materials under 808 nm excitation, polycrystalline powders of $GdVO_4:Er^{3+}/Nd^{3+}$ and $GdVO_4:Ho^{3+}/Nd^{3+}$ were successfully prepared by a high-temperature solid-state reaction technique. The prepared powders were highly crystalline with a single-phase zircon-type $GdVO_4$ structure and consisted of micrometer-sized irregular spherical particles (2–6 μm in diameter). In all studied samples, visible up-conversion luminescence was successfully achieved under 808 nm illumination. Near-infrared pumping produced emission bands in the green, yellow-orange and green regions of the visible spectrum. The bands in the green and red regions of $GdVO_4:Er^{3+}/Nd^{3+}$ as well as $GdVO_4:Ho^{3+}/Nd^{3+}$ were, respectively, characteristic of Er^{3+} and Ho^{3+} ions. The dominant band originating from the $^4G_{7/2} \rightarrow {}^4I_{11/2}$ transition in Nd^{3+} ions was observed around 597 nm in all samples.

1. Introduction

Up-conversion (UC) luminescence is a unique anti-Stokes process where low-energy excitation light, usually near-infrared (NIR) light, is converted to higher-energy (NIR or visible/ultraviolet (Vis/UV)) light through sequential absorption of multiple photons or energy transfers. In recent years, up-converting materials, lanthanide-doped inorganic materials emitting NIR-to-NIR or NIR-to-Vis/UV UC luminescence caused by NIR light illumination, have received much attention. Typically, these phosphors are made of low phonon energy host materials which are double-doped with sensitizer ions (usually Yb^{3+}) and activator ions (Er^{3+}, Tm^{3+}, or Ho^{3+} in most cases). With the advent of nanotechnology and the inexpensive high-power infrared diode lasers, UC nanoparticles (UCNPs) have found many uses including, but not limited to, solar energy conversion, sensing and, in particular, a variety of biomedical applications [1–3].

Compared with conventional (down-conversion) phosphors excited by UV/Vis light, UCNPs used in biomedicine exhibit numerous advantages, such as lower autofluorescence background, excellent photostability, negligible photoblinking, less scattering and absorption, and deeper penetration into biological samples. Ytterbium (Yb^{3+})-sensitized UCNPs have been commonly used, and a 980 nm excitation is required to trigger the UC process; Yb^{3+} ions have a very narrow absorption band at about that wavelength and they can efficiently transfer excitation energy to Er^{3+}, Ho^{3+} or Tm^{3+} ions. However, using an excitation source of 980 nm in biomedical applications has an intrinsic disadvantage: water, as a principle constituent of biological materials, exhibits a strong absorption in the 900–1000 nm spectral region. The absorption attenuates excitation light passing through tissues which results in a shorter penetration, while absorbed light converted into heat induces local heating and may lead to overheating of cells or tissues in conjunction with substantial cell and tissue damage [1–6].

Shifting the excitation to shorter wavelengths, in particular, making use of 808 nm excitation, may both overcome the overheating issues and improve the penetration depth. At this wavelength, water absorption is much lower (the absorption coefficient is 0.02 cm^{-1} at 808 nm, in contrast to 0.48 cm^{-1} at 980 nm), light penetrates deeper into tissues and tissues heat up slower [5]. In order to shift the excitation to shorter wavelengths, first, the Yb^{3+} ions have been replaced by suitable NIR organic sensitizers. However, unlike UCNPs, organic dyes are susceptible to photobleaching, thus making these NIR dye-sensitized UCNPs unsuitable for a long-term usage. Recently, novel materials capable of producing UC luminescence under NIR excitation at 808 nm have come to prominence. Yb^{3+} ions and dyes have been superseded by ions of neodymium (Nd^{3+}) ions, as sensitizers into a typical sensitizer/

* Corresponding author.
E-mail address: draganaj@vinca.rs (D.J. Jovanović).

https://doi.org/10.1016/j.optmat.2018.05.033
Received 28 February 2018; Received in revised form 9 May 2018; Accepted 11 May 2018

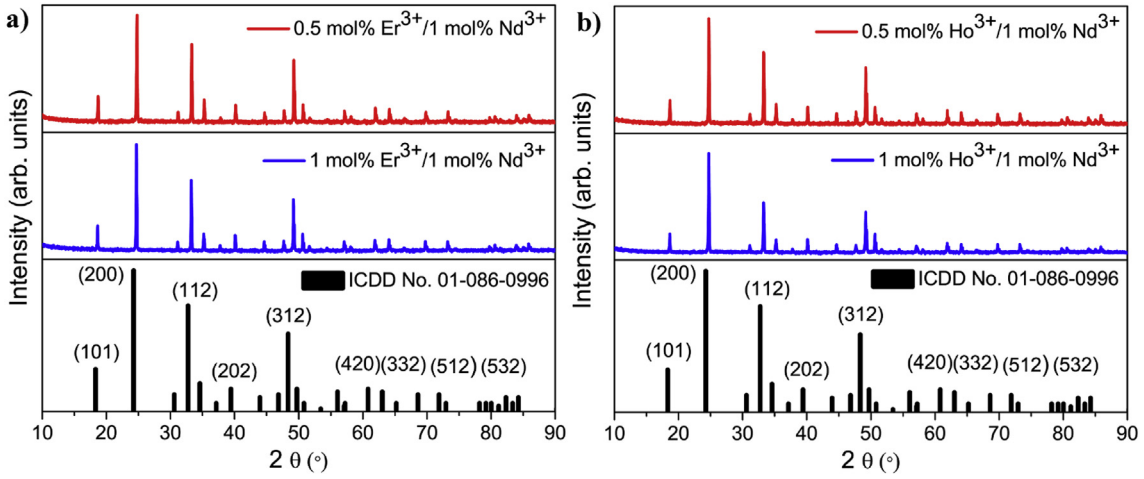

Fig. 1. XRD patterns of: a) Er^{3+}/Nd^{3+}- and b) Ho^{3+}/Nd^{3+} -doped $GdVO_4$ samples. Vertical bars denote the standard data for tetragonal zircon-type phase of bulk $GdVO_4$ (ICDD card No. 01-086-0996).

activator UC system, assume the role of Yb^{3+} ions as the main NIR absorber [4–6].

Gadolinium orthovanadate ($GdVO_4$) is a well-established host matrix used in preparation of various optical materials. These materials are utilized in many applications, such as solid-state laser hosts, polarizers, phosphors, cathode ray tubes, dye-sensitized solar cells, photovoltaic cells, laser diode pumped micro-lasers, and bio-probes [7–10]. Good down-conversion performance of lanthanide-doped $GdVO_4$ could be attributed to the strong UV absorption of the VO_4^{3-} groups and efficient energy transfer from the matrix to activator ions. $GdVO_4$ also seems to be a promising host for phosphors which can be excited by NIR radiation because its high chemical stability, close lattice matches to dopant ions and comparatively low phonon energy. There are a dozen or so studies concerning successful preparation of Yb^{3+}-sensitized $GdVO_4$-based materials, mostly double-doped and nanostructured: $GdVO_4$:Yb^{3+}/Er^{3+} [7,8,11–19], $GdVO_4$:Yb^{3+}/Ho^{3+} [8,12,16,18,19] and $GdVO_4$:Yb^{3+}/Tm^{3+} [8,12,16,18–20]. Nothing about double-doped $GdVO_4$ excited at 808 nm, particularly about Nd^{3+}-sensitized $GdVO_4$-based materials, has been reported before.

Herein, in order to further our earlier work on up-converting lanthanide-doped $GdVO_4$ phosphors [7,8,10,15], $GdVO_4$:Nd^{3+}/Er^{3+} and $GdVO_4$:Nd^{3+}/Ho^{3+} systems were synthesized using a high temperature solid-state reaction technique. The main aim was to produce UC luminescence emission of these materials under 808 nm excitation.

2. Experimental

2.1. Materials and methods

Four $GdVO_4$-based samples, $GdVO_4$:x mol%Ho^{3+}/1mol%Nd^{3+} and $GdVO_4$:x mol%Er^{3+}/1mol%Nd^{3+} (x = 0.5 and 1), were synthesized by high-temperature solid-state techniques. All chemicals: gadolinium (III) oxide, Gd_2O_3 (99.99%, Alfa Aesar), holmium (III) oxide, Ho_2O_3 (99.99%, Alfa Aesar), erbium (III) oxide, Er_2O_3 (99.99%, Alfa Aesar), neodymium (III) oxide, Nd_2O_3 (99.99%, Alfa Aesar), ammonium vanadate, NH_4VO_3 (Alfa Aesar, 99.999%), sodium hydroxide and methanol were of the highest purity commercially available and were used without further purification.

In a typical synthesis, the starting materials Gd_2O_3, Er_2O_3 or Ho_2O_3, Nd_2O_3 and NH_4VO_3 in appropriate stoichiometric ratio were homogeneously mixed by dry grinding and then heated in open crucibles at three different temperature. First, a grounded mixture of precursors was heated from room temperature up to temperature of 800 °C and kept at this temperature for 1 h. Next, the product was removed from the furnace, cooled down to room temperature, ground and, in order to complete the reaction, once reheated at 1100 °C for another 3 h. After that, the resulting powder was ground homogeneously, and three times washed and centrifuged using 2 M NaOH, water and methanol, respectively. At the end, the reaction product was additionally calcined at 1150 °C for 90 min to improve crystallinity and remove ligands attached to the particle surfaces during washing.

Additionally, $GdVO_4$:12mol%Nd^{3+} sample was prepared in the same manner as above, its phase purity were confirmed by XRD analysis and this sample was used in analysis of diffuse reflection spectra (see Section 3.2.1).

2.2. Instruments

Powder X-ray diffraction (XRD) measurements were performed on a Rigaku SmartLab diffractometer using Cu-$K_{\alpha 1,\ 2}$ radiation (λ = 0.15405 nm). Diffraction data were recorded with a step size of 0.01° and a counting time of 1 deg/min over the 2θ range of 10°–90°. Microstructural characterization was performed on a JEOL JSM-6610LV scanning electron microscope (SEM).

Diffuse reflection spectra measurements were recorded with 1 nm resolution on a Shimadzu UV-Visible UV-2600 (Shimadzu Corporation, Japan) spectrophotometer equipped with an integrated sphere (ISR-2600 Plus (for UV-2600)) in the range from 230 nm to 1350 nm. Luminescence measurements were performed using a Andor Shamrock B-303i spectrograph coupled with a CCD camera (Andor DU-401A-BV) at exit port (Input side slit width: 100 μm, spectral range: 500–715 nm). The excitation source was 808 nm Multimode Laser Diode from Thorlabs operating at 1000 mW. A pulsed solid state laser NT342/3UV (pulse duration ~ 5ns) from Ekspla (tunable wavelength from 210 nm to 2300 nm, linewidth is 4.3 cm^{-1}) was used for luminescence kinetics measurements. Luminescence spectra were recorded by an ICCD camera (Andor iSTAR DH734_18 mm) coupled to Andor SR-303i-B monochromator/spectrometer. Luminescence decay kinetics were obtained as a series of delayed luminescence spectra recorded after the excitation laser pulse (Exposure time: 0.045 s, gate delay: 50 ns, spectral range: 500–700 nm).

3. Results and discussions

3.1. Structural and microstuctural properties

In Fig. 1 are given X-ray diffraction patterns of all the samples together with ICDD card No. 01-086-0996 data indicating the presence of a single tetragonal zircon-type phase of $GdVO_4$ (space group I41/amd). In the zircon-type crystal lattice, Gd^{3+} ions (with D_{2d} point symmetry)

Table 1
Lattice parameters and average crystallite size for all synthesized $GdVO_4$:xmol% Er^{3+}/1 mol%Nd^{3+} and $GdVO_4$:xmol% Ho^{3+}/1 mol%Nd^{3+} (x = 0.5 or 1) samples.

Samples ($GdVO_4$:1mol% Nd^{3+}/)	0.5mol% Er^{3+}	1mol% Er^{3+}	0.5mol% Ho^{3+}	1mol% Ho^{3+}
a = b (Å)	7.21201	7.2114	7.2135	7.2133
c (Å)	6.34819	6.3479	6.3497	6.3501
Crystallite size (nm)	47.7	63.9	57.8	61.3

are located within a distorted dodecahedron of eight O^{2-} ions, while V^{5+} ions in the $[VO_4]^{3-}$ groups are tetrahedrally coordinated with O^{2-} ions. The absence of impurity phases and very small shift of reflections compared to the reflection positions of pure $GdVO_4$ indicate that Er^{3+} (Ho^{3+}) and Nd^{3+} ions were successfully and uniformly incorporated into the $GdVO_4$ host lattice at substitutional sites due to similar ionic radii and ionic charges of the dopant and Gd^{3+} ions. Relatively intense reflection peaks were observed suggesting that the samples (calcined at 1150 °C for 90 min) were highly crystalline and that no further thermal treatment was required. The diffraction patterns clearly shows a strong (2 0 0) preferred orientation in all the samples.

All structural parameters (average crystal size, unit cell parameters and strain) of the Er^{3+}/Nd^{3+}- and Ho^{3+}/Nd^{3+}-doped $GdVO_4$ were estimated by the Halder-Wagner method and by structural Rietveld refinement (see Table 1). Calculated values of crystallite size are in range from 48 to 64 nm, while microstrain values (which are not listed in Table 1), are from 0.03 to 0.11% suggesting a good ions ordering in the nanocrystals.

Fig. 2 shows SEM images of the microstructure of the doped $GdVO_4$ samples at different magnifications. The materials were comprised of chunks of irregular spherical (deformed) particles with an average diameter ranging from approximately 2 μm–6 μm. Note that difference in doping concentrations of Er^{3+} or Ho^{3+} exhibited no effect on the morphology and crystal structure of $GdVO_4$.

3.2. Optical properties

3.2.1. Diffuse reflection spectra

UV-Vis-NIR diffuse reflection spectra at room temperature of the Er^{3+}/Nd^{3+}- and Ho^{3+}/Nd^{3+}-doped $GdVO_4$ powders are given in Fig. 3. In order to facilitate their analysis, diffuse reflection spectrum of the $GdVO_4$:Nd^{3+} powder was also recorded and presented. Wavelengths of the band positions (marked with numbers and letters in the spectra) along with corresponding transitions are listed in Table 2.

All analyzed materials showed strong absorption in the UV spectral region. As is well-known, the strong UV absorption of vanadate materials may be attributed a V^{5+}-O^{2-} charge transfer from the excited oxygen ligands (O^{2-}) to the central vanadium atom (V^{5+}) in the VO_4^{3-} groups. According to the molecular orbital theory, this corresponds to transitions from the $^1A_2(^1T_1)$ ground state to the $^1A_1(^1E)$ and $^1E(^1T_2)$ excited states of the VO_4^{3-} ions, i.e., in crystalline $GdVO_4$, the original T_d symmetry of VO_4^{3-} (free ion) is reduced to D_{2d} by the crystal field; this causes a splitting of the degenerate levels of VO_4^{3-} [7].

Sharp narrow absorption bands of the $GdVO_4$:Nd^{3+} sample were observed in the range from ~450 nm to ~900 nm, and, apart from these bands, additional absorption bands appeared in the spectra of $GdVO_4$:Er^{3+}/Nd^{3+} and $GdVO_4$:Ho^{3+}/Nd^{3+} powders. The absorption bands (see Fig. 3 and Table 2) of Nd^{3+}, Er^{3+} and Ho^{3+} could be attributed to the intra-configurational f-f electronic transitions from the ground levels $^4I_{9/2}$, $^4I_{15/2}$ and $^5I_8$ respectively to various excited states [21–23]. Electric dipole transitions between 4f levels, involving no change in parity, only occur because of interaction with the crystal field of host lattice causes mixing of electronic states. Magnetic dipole transitions between 4f levels are allowed, but, usually, their intensity is weak. For our purposes it is important that absorption at 808 nm, which results from Nd^{3+}: $^4I_{9/2}\rightarrow{}^4F_{5/2}$, $^2H_{9/2}$, was present in all the spectra.

$GdVO_4$ is a direct band gap material with band gap energy E_g = 3.57 eV [24]. To estimate the band gap energy of $GdVO_4$:Er^{3+}/Nd^{3+} and $GdVO_4$:Ho^{3+}/Nd^{3+} from the diffuse reflection spectra, the Kubelka–Munk theory was used [7,24]. The band gap E_g value was determined by extrapolating the steepest portion of the graph on the

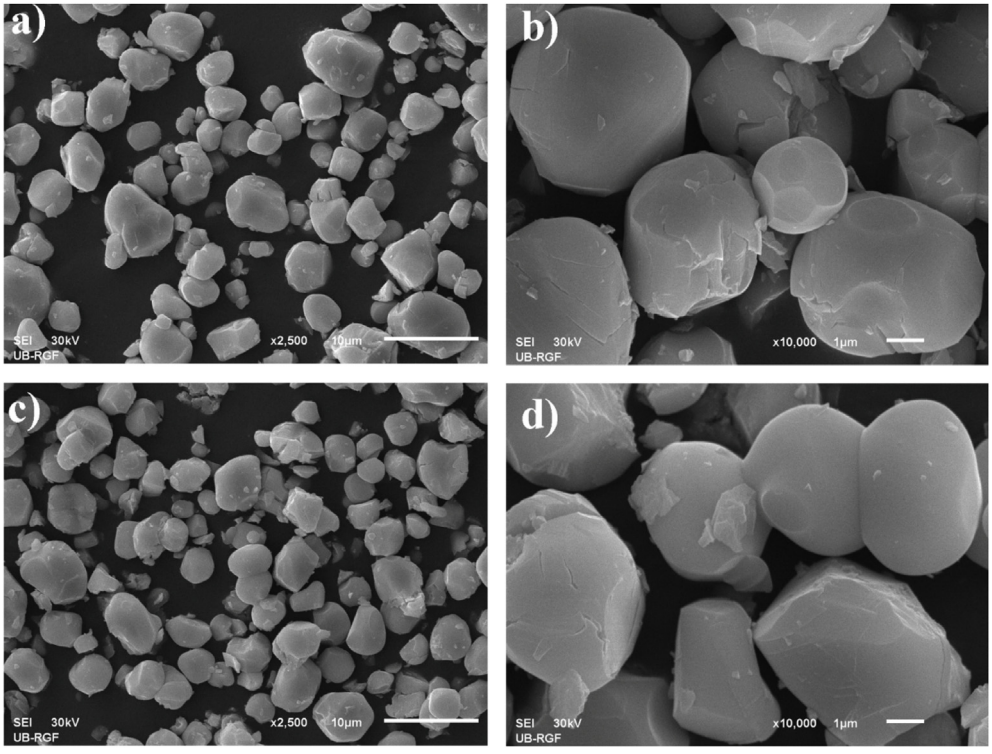

Fig. 2. SEM images of: (a, b) Er^{3+}/Nd^{3+}- and (c, d) Ho^{3+}/Nd^{3+}-doped $GdVO_4$ samples at different magnifications.

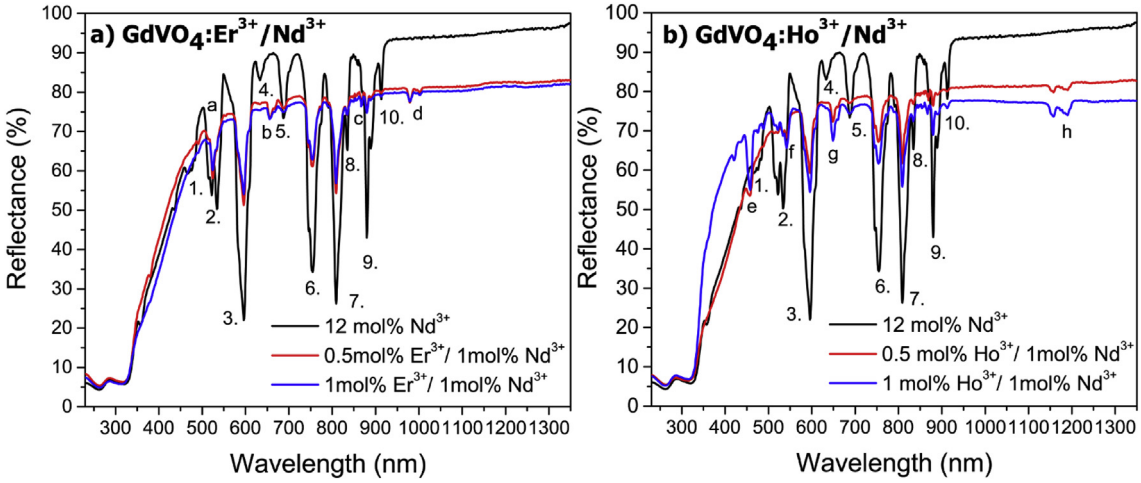

Fig. 3. Diffuse reflection spectra of: a) Er^{3+}/Nd^{3+}- and b) Ho^{3+}/Nd^{3+}-doped $GdVO_4$ samples. For the sake of comparison, spectra of Nd^{3+}-doped $GdVO_4$ are depicted in black.

Table 2
Absorption band positions and corresponding transitions from diffuse reflection spectra of Nd^{3+}-, Er^{3+}/Nd^{3+}- and Ho^{3+}/Nd^{3+}-doped $GdVO_4$ samples.

Ion	Band	Wavelength (nm)	Transition
Nd^{3+}	1.	468	$^4I_{9/2}\rightarrow{}^4G_{9/2}$
	2.	521/535	$^4I_{9/2}\rightarrow{}^4G_{7/2},{}^4G_{9/2}$
	3.	596	$^4I_{9/2}\rightarrow{}^4G_{5/2},{}^4G_{7/2}$
	4.	634	$^4I_{9/2}\rightarrow{}^2H_{11/2}$
	5.	685	$^4I_{9/2}\rightarrow{}^4F_{9/2}$
	6.	753	$^4I_{9/2}\rightarrow{}^4F_{7/2},{}^4S_{3/2}$
	7.	808	$^4I_{9/2}\rightarrow{}^4F_{5/2},{}^2H_{9/2}$
	8.	833	$^4I_{9/2}\rightarrow{}^4F_{5/2},{}^2H_{9/2}$
	9.	881	$^4I_{9/2}\rightarrow{}^4F_{3/2}$
	10.	915	$^4I_{9/2}\rightarrow{}^4F_{3/2}$
Er^{3+}	a	524	$^4I_{15/2}\rightarrow{}^2H_{11/2}$
	b	655	$^4I_{15/2}\rightarrow{}^4F_{9/2}$
	c	864	$^4I_{15/2}\rightarrow{}^4I_{9/2}$
	d	980/1004	$^4I_{15/2}\rightarrow{}^4I_{11/2}$
Ho^{3+}	e	456	$^5I_8\rightarrow{}^5G_6$
	f	544	$^5I_8\rightarrow{}^5S_2,{}^5F_4$
	g	647	$^5I_8\rightarrow{}^5F_5$
	h	1152/1191	$^5I_8\rightarrow{}^5I_6$

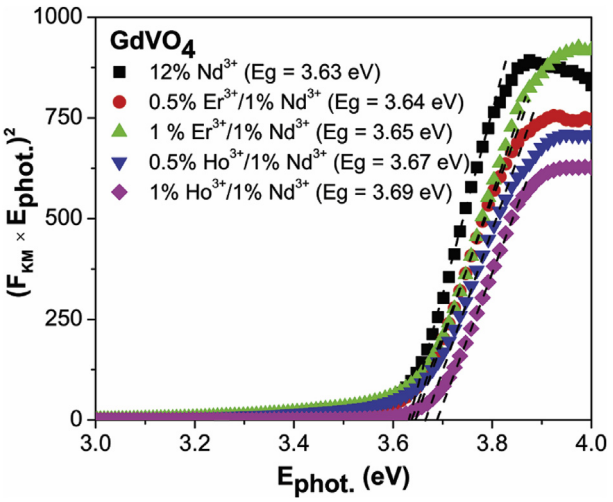

Fig. 4. Band gap energy values, E_g (eV), calculated from diffuse reflection spectra. All the studied samples together with $GdVO_4$:12%Nd^{3+} are considered.

E_{phot} axis at $(F_{KM} \times E_{phot.})^2 = 0$ as it is shown in Fig. 4. The estimated band gap values in the range from 3.63 eV up to 3.69 eV are in full agreement with recently published results for $GdVO_4$. Note a small blue-shift for the absorption edge of double-doped $GdVO_4$ due to influence of doping (see Fig. 4).

3.2.2. Up-conversion luminescence under 808 nm excitation

Fig. 5 shows visible luminescence emission under 808 nm excitation of $GdVO_4$:Nd^{3+}/Er^{3+} and $GdVO_4$: Nd^{3+}/Ho^{3+} recorded at room temperature. For all the samples, three or four bands in luminescence spectra were observed, each containing multiple peaks.

In case of $GdVO_4$:Nd^{3+}/Er^{3+}, luminescence emission was found in the ranges 520–565 nm, 570–630 nm and 640–680 nm. Spectra of different samples are similar in shape, there is no shift in the peak positions but there is a change in the intensity of the peaks. The observed green and red emissions around 525 nm, 550 nm and 675 nm are consistent with the well-known electronic transitions to the ground state level $^4I_{15/2}$ from higher levels in Er^{3+} ions: $^2H_{11/2}\rightarrow{}^4I_{15/2}$, $^4S_{3/2}\rightarrow{}^4I_{15/2}$ and $^4F_{9/2}\rightarrow{}^4I_{15/2}$, respectively [21,23]. The luminescence centred on 597 nm should be attributed to the transition $^4G_{7/2}\rightarrow{}^4I_{11/2}$ in Nd^{3+} ions [23,24]. In case of $GdVO_4$:Nd^{3+}/Ho^{3+}, three luminescence bands were observed. Again, spectra of different samples are similar in shape with no apparent change in the peak positions, but they differ in luminescent intensity. The dominant 597-nm emission is characteristic of the $^4G_{7/2}\rightarrow{}^4I_{11/2}$ transition in Nd^{3+} ions [23,24], while other bands could be due to electronic transitions to the ground state level $^5I_8$ from higher levels in Ho^{3+} ions: $^5F_4$, $^5S_2\rightarrow{}^5I_8$ (540 nm) and $^5F_5\rightarrow{}^5I_8$ (659 nm) [22,26].

Clearly, 808-nm excited upconversion was achieved in all the double-doped $GdVO_4$ samples, however, the determination of the governing mechanism behind luminescence is not at all straightforward. In general, changing the host materials (differing the phonon energy) may substantially influence the multi-phonon relaxation as well as energy transfer process, which may lead to an entirely different upconversion luminescence behavior. It is well-known that around 800 nm, absorption cross section of Nd^{3+} is relatively high, while commonly used activators (Er^{3+}, Tm^{3+}, and Ho^{3+}) and sensitizer (Yb^{3+}) exhibit extremely low-absorption cross section. Also, it is known that Nd^{3+} can produce UC luminescence in single-doped 808 nm-excited materials [25,27]. However, it was reported that Er^{3+} and Ho^{3+} ions also show visible UC luminescence under 808 excitation in certain single-doped host lattices [28,29]. Here, the presence of emission lines from erbium/holmium and neodymium ions in the luminescence spectra of Nd^{3+}/Er^{3+}-doped $GdVO_4$ and Nd^{3+}/Ho^{3+}-doped $GdVO_4$ indicates a multistage energy transfer between active centers. The Nd^{3+}

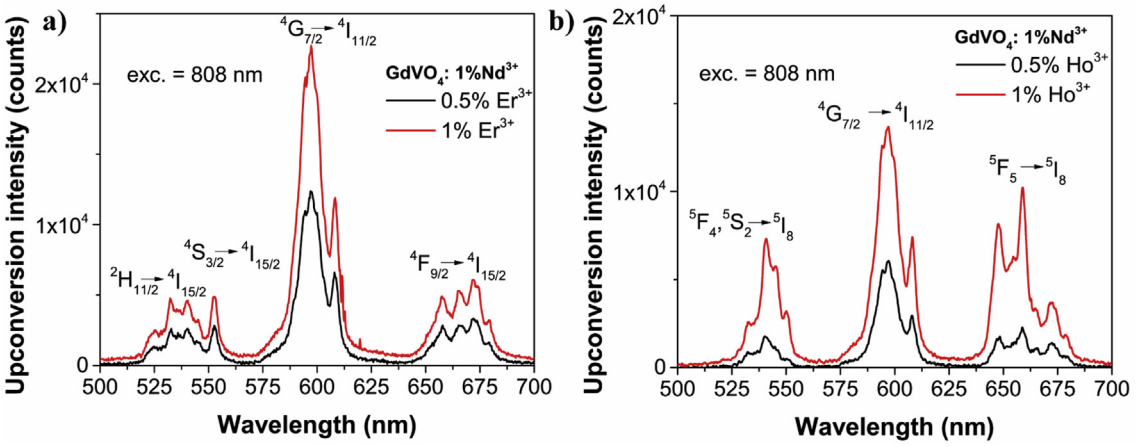

Fig. 5. Visible UC luminescence emission spectra of: a) Er^{3+}/Nd^{3+}- and b) Ho^{3+}/Nd^{3+}-doped $GdVO_4$ samples.

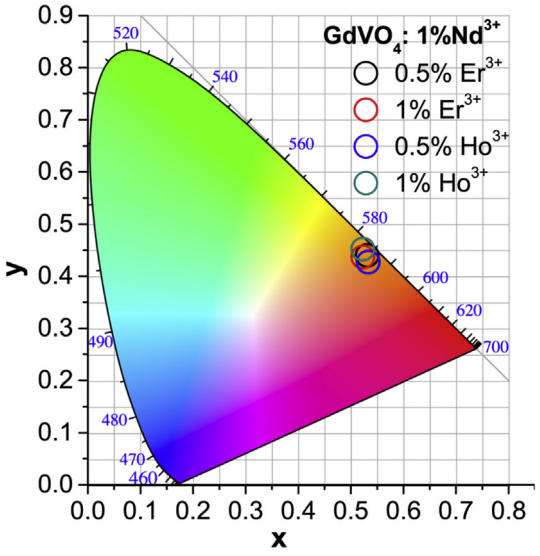

Fig. 6. CIE coordinates of the UC luminescence color for all the studied phosphors. (For interpretation of the references to color in this figure legend, the reader is referred to the Web version of this article.)

emission at about 597 nm, which dominated in all the spectra, is particularly interesting and an increase of its intensity with increasing of the number of Er^{3+}/Ho^{3+} ions could be associated with efficient Er^{3+}/Ho^{3+}- Nd^{3+} energy transfer. The above results definitely confirmed UC luminescence (λ_{exc} = 808 nm), but possible mechanisms of the energy transfer processes between ions and how our findings can be interpreted certainly requires further investigation.

An average lifetime for all samples and all emission maxima were estimated using the following equation: $\tau_{avg.} = \int_0^\infty tI(t)dt / \int_0^\infty I(t)dt$, where *I(t)* represents the luminescence intensity at time *t* corrected for the background; the integrals were evaluated in the range $0 < t < t_m$ where $t_m \ll \tau_{avg}$ [30]. Calculated average lifetime values for all the samples under excitation at 808 nm were in the range from 13 up to 35 μs for the samples $GdVO_4$:1mol%Nd^{3+}/1mol%Ho^{3+} and $GdVO_4$:1mol%Nd^{3+}/0.5mol%Er^{3+}, respectively.

For visualization of the color of emitted light from the samples the color coordinates were determined and are shown in the CIE chromaticity diagram in Fig. 6. The calculated color coordinates (x, y) for investigated materials were calculated to be as follows: (0.531, 0.440) $GdVO_4$:1%Nd^{3+}/0.5%Er^{3+}, (0.523, 0.437) $GdVO_4$:1%Nd^{3+}/1%Er^{3+}, (0.533, 0.427) $GdVO_4$:1%Nd^{3+}/0.5%Ho^{3+} and (0.523, 0.452) $GdVO_4$:1%Nd^{3+}/1%Ho^{3+}.

4. Conclusions

It could be concluded from the literature that Yb^{3+}-sensitized $GdVO_4$-based materials, including $GdVO_4$:Yb^{3+}/Er^{3+}, $GdVO_4$:Yb^{3+}/Ho^{3+} and $GdVO_4$:Yb^{3+}/Tm^{3+}, are rather well studied. These powders with particles of sizes ranging from several nanometers to several micrometers have been prepared by verious synthetic techniques and they exhibit UC luminescence emission under excitation at 980 nm. However, it appears that optical properties of double-doped $GdVO_4$ systems under 808 nm excitation were not studied at all before.

Double-doped $GdVO_4$-based polycrystalline powders, $GdVO_4$:xmol%Ho^{3+}/1mol%Nd^{3+} and $GdVO_4$:xmol%Er^{3+}/1mol%Nd^{3+} (x = 0.5 and 1), were successfully prepared by a high-temperature solid-state reaction technique. The obtained materials consisting of micrometer-sized irregular spherical particles (2–6 μm in diameter) were highly crystalline and a single tetragonal zircon-type phase of $GdVO_4$ (space group I41/amd) was confirmed in all samples.

By making use of an inexpensive laser diode (1 W) as an excitation source, UC luminescence emission (recorded in the 500–715 nm range) was successfully achieved in all the samples under 808 nm illumination. NIR pumping produced emission bands in the green, yellow-orange and red regions of the visible spectrum. In all studied materials, the dominant band originating from the $^4G_{7/2} \rightarrow {}^4I_{11/2}$ transition in Nd^{3+} ions was observed around 597 nm. The bands in the green and red regions of $GdVO_4$: Er^{3+}/Nd^{3+} as well as $GdVO_4$:Ho^{3+}/Nd^{3+} were, respectively, characteristic of Er^{3+} and Ho^{3+} ions. These initial results of an ongoing research certainly require further investigation.

Acknowledgements

All authors acknowledge to the COST Action CM1403: The European upconversion network - from the design of photon-upconverting nanomaterials to biomedical applications (2014–2018). The authors from the University of Belgrade acknowledge the financial support of the Ministry of Education, Science and Technological Development of the Republic of Serbia (Project Nos. 45020 and 172056). K. S. acknowledges the Latvian National Research Program IMIS2 (Grant No. 302/2012). T. G. acknowledges the ERDF PostDoc project No. 1.1.1.2/VIAA/1/16/215 (1.1.1.2/16/I/001).

References

[1] J. Zhou, Q. Liu, W. Feng, Y. Sun, F. Li, Upconversion luminescent materials: advances and applications, Chem. Rev. 115 (2015) 395–465.
[2] S. Wang, H. Zhang, Chapter 7, foundations of up-conversion nanoparticles, in: R.-

S. Liu (Ed.), Phosphors, up Conversion Nano Particles, Quantum Dots and Their Applications, vol. 2, Springer, 2016.
[3] G.-R. Tan, M. Wang, C.-Y. Hsu, N. Chen, Y. Zhang, Small upconverting fluorescent nanoparticles for biosensing and bioimaging, Adv. Opt. Mater. 4 (2016) 984–997.
[4] M.K.G. Jayakumar, N.M. Idris, K. Huang, Y. Zhang, A paradigm shift in the excitation wavelength of upconversion nanoparticles, Nanoscale 6 (2014) 8441–8143.
[5] Y.-F. Wang, G.-Y. Liu, L.-D. Sun, J.-W. Xiao, J.-C. Zhou, C.-H. Yan, Nd^{3+}-sensitized upconversion nanophosphors: efficient in vivo bioimaging probes with minimized heating effect, ACS Nano 7 (2013) 7200–7206.
[6] X. Xie, Z. Li, Y. Zhang, S. Guo, A.I. Pendharkar, M. Lu, L. Huang, W. Huang, G. Han, Emerging ≈800 nm excited lanthanide-doped upconversion nanoparticles, Small 13 (2017) 1602843 (15 pp).
[7] T.V. Gavrilović, D.J. Jovanović, V. Lojpur, M.D. Dramićanin, Multifunctional Eu^{3+} and Er^{3+}/Yb^{3+}-doped $GdVO_4$ nanoparticles synthesized by reverse micelle method, Sci. Rep. 4 (2014) 4209.
[8] T.V. Gavrilović, D.J. Jovanović, K. Smits, M.D. Dramićanin, Multicolor upconversion luminescence of $GdVO_4$:Ln^{3+}/Yb^{3+} (Ln^{3+} = Ho^{3+}, Er^{3+}, Tm^{3+}, $Ho^{3+}/Er^{3+}/Tm^{3+}$) nanorods, Dyes Pigments 126 (2016) 1–7.
[9] K. Dong, E. Ju, J. Liu, X. Han, J. Ren, X. Qu, Ultrasmall biomolecule-anchored hybrid $GdVO_4$ nanophosphors as a metabolizable multimodal bioimaging contrast agent, Nanoscale 6 (2014) 12042–12049.
[10] T.V. Gavrilović, D.J. Jovanović, L.V. Trandafilović, M.D. Dramićanin, Effects of Ho^{3+} and Yb^{3+} doping concentrations and Li^+ co-doping on the luminescence of $GdVO_4$ powders, Opt. Mater. 45 (2015) 76–81.
[11] Y. Liang, H.M. Noh, J. Xue, H. Choi, S.H. Park, B.C. Choi, J.H. Kim, J.H. Jeong, High quality colloidal $GdVO_4$:Yb,Er upconversion nanoparticles synthesized via a protected calcination process for versatile applications, Mater. Des. 130 (2017) 190–196.
[12] A. Tymiński, T. Grzyb, S. Lis, $REVO_4$ -based nanomaterials (RE = Y, La, Gd, and Lu) as hosts for Yb^{3+}/Ho^{3+}, Yb^{3+}/Er^{3+} and Yb^{3+}/Tm^{3+} ions: structural and up-conversion luminescence studies, J. Am. Ceram. Soc. 99 (2016) 3300–3308.
[13] O.A. Savchuk, J.J. Carvajal, C. Cascales, M. Aguiló, F. Díaz, Benefits of silica core–shell structures on the temperature sensing properties of Er,Yb:$GdVO_4$ up-conversion nanoparticles, ACS Appl. Mater. Interfaces 8 (2016) 7266–7273.
[14] J.H. Oh, B.K. Moon, B.C. Choi, J.H. Jeong, J.H. Kim, H.S. Lee, The green upconversion emission mechanism investigation of $GdVO_4$:Yb^{3+},Er^{3+} via tuning of the sensitizer concentration, Solid State Sci. 42 (2015) 1–5.
[15] T.V. Gavrilović, D.J. Jovanović, V.M. Lojpur, V. Đorđević, M.D. Dramićanin, Enhancement of luminescence emission from $GdVO_4$:Er^{3+}/Yb^{3+} phosphor by Li^+ co-doping, J. Solid State Chem. 217 (2014) 92–98.
[16] X. Kang, D. Yang, Y. Dai, M. Shang, Z. Cheng, X. Zhang, H. Lian, P. Ma, J. Lin, Poly (acrylic acid) modified lanthanide-doped $GdVO_4$ hollow spheres for up-conversion cell imaging, MRI and pH-dependent drug release, Nanoscale 5 (2013) 253–261.
[17] V. Mahalingam, C. Hazra, R. Naccache, F. Vetrone, J.A. Capobianco, Enhancing the color purity of the green upconversion emission from Er^{3+}/Yb^{3+}-doped $GdVO_4$ nanocrystals via tuning of the sensitizer concentration, J. Mater. Chem. C 1 (2013) 6536–6540.
[18] W. Yin, L. Zhou, Z. Gu, G. Tian, S. Jin, L. Yan, X. Liu, G. Xing, W. Ren, F. Liu, Z. Pan, Y. Zhao, Lanthanide-doped $GdVO_4$ upconversion nanophosphors with tunable emissions and their applications for biomedical imaging, J. Mater. Chem. 22 (2012) 6974–6981.
[19] R. Calderon-Villajos, C. Zaldo, C. Cascales, Enhanced upconversion multicolor and white light luminescence in SiO_2-coated lanthanide-doped $GdVO_4$ hydrothermal nanocrystals, Nanotechnology 23 (2012) 505205 (10pp).
[20] H.K. Yang, S.J. Park, J.Y. Park, J.-Y. Je, Influence of the variation Yb^{3+} concentration and sintering temperature in $GdVO_4$: Tm^{3+}/Yb^{3+} blue emission phosphors, Optik 131 (2017) 475–482.
[21] P. Wang, H. Xia, J. Peng, H. Hu, L. Tang, Y. Zhang, B. Chen, H. Jiang, Concentration effect of Nd^{3+} ion on the spectroscopic properties of Er^{3+}/Nd^{3+} co-doped $LiYF_4$ single crystal, Mater. Chem. Phys. 144 (2014) 349–354.
[22] J. Qiuy, M. Shojiyay, R. Kannoy, Y. Kawamotoy, M. Takahashi, Selectively strong green up-conversion luminescence in co-doped -based fluoride glasses under 800 nm excitation, J. Phys. Condens. Matter 10 (1998) 11095–11102.
[23] Y. Xu, J. Qi, J. Ren, G. Chen, F. Huang, Y. Li, S. Lu, S. Dai, Luminescence and energy transfer in Er^{3+}/Nd^{3+} ion-codoped Ge–In–S–CsBr chalcohalide glasses, Mater. Res. Bull. 48 (2013) 4733–4737.
[24] P. Kumari, J. Manam, Structural, optical and special spectral changes of Dy^{3+} emissions in orthovanadates, RSC Adv. 5 (2015) 107575.
[25] X.D. Li, X. Yu, J. Gao, F. Chen, J.H. Yu, D.Y. Chen, Upconversion spectra of Nd:$GdVO_4$ crystal under CW 808 nm diode-laser pumping, Laser Phys. Lett. 6 (2009) 125–128.
[26] J. Yuan, S.X. Shen, D.D. Chen, Q. Qian, M.Y. Peng, Q.Y. Zhang, Efficient 2.0 μm emission in Nd^{3+}/Ho^{3+} co-doped tungsten tellurite glasses for a diode pump 2.0 μm laser, J. Appl. Phys. 113 (2013) 173507.
[27] Near-infrared-to-near-infrared down-shifting and upconversion luminescence of KY_3F_{10} with single dopant of Nd^{3+} ion, Appl. Phys. Lett. 108 (2016) 041902.
[28] R. Lisiecki, W. Ryba-Romanowski, E. Cavalli, M. Bettinelli, Optical spectroscopy of Er^{3+}-doped $LaVO_4$ crystal, J. Lumin. 130 (2010) 131–136.
[29] S.-Y. Liao, R. Yao, Y.-C. Liu, X.-Y. Chen, X.-Y. Hua, F. Zheng, Green up-conversion of C12A7–Ho^{3+} prepared by co-precipitation method, J. Alloy. Comp. 642 (2015) 7–14.
[30] S. Shionoya, W.M. Yen, Phosphor Handbook, CRC Press LLC, Boca Raton, 1999.